Table S1 List of exchanged variables in CAPS with the original coupling approach.

Variable	Source	Destination	Meaning
F_{swdn}	WRF	ROMS, CICE	Downward shortwave radiation at the surface
F_{lwdn}	WRF	ROMS, CICE	Downward longwave radiation at the surface
T_{2m}	WRF	ROMS, CICE	Air temperature at 2 m height
Q_{2m}	WRF	CICE	Specific humidity at 2 m height
RH	WRF	ROMS	Relative humidity at 2 m height
$\vec{U}_{10m}$	WRF	ROMS, CICE	Wind fields at 10 m height
$\vec{\tau}_{ao}$	WRF	ROMS	Wind stress at the atmosphere–ocean interface
$MSLP$	WRF	ROMS	Mean sea level pressure
P_{total}	WRF	ROMS, CICE	Total precipitation rate
E_{ao}	WRF	ROMS	Evaporation rate at the atmosphere–ocean interface
SST	ROMS	WRF, CICE	Sea surface temperature
SSS	ROMS	CICE	Sea surface salinity
W_{fr}	ROMS	CICE	Freezing/melting potential
$\vec{U}_o$	ROMS	CICE	Surface ocean currents
∇H_o	ROMS	CICE	Sea surface slope
A_{ice}	CICE	WRF	Sea ice concentration
T_{ice}	CICE	WRF	Ice surface temperature
α_{ice}	CICE	WRF	Surface albedo of snow and ice
$F_{swthru,io}$	CICE	ROMS	Penetrated shortwave radiation through sea ice
$F_{heat,io}$	CICE	ROMS	Net heat flux at the ice–ocean interface
$F_{water,io}$	CICE	ROMS	Freshwater flux at the ice–ocean interface
$F_{salt,io}$	CICE	ROMS	Salt flux at the ice–ocean interface
$\vec{\tau}_{io}$	CICE	ROMS	Ice–ocean stress

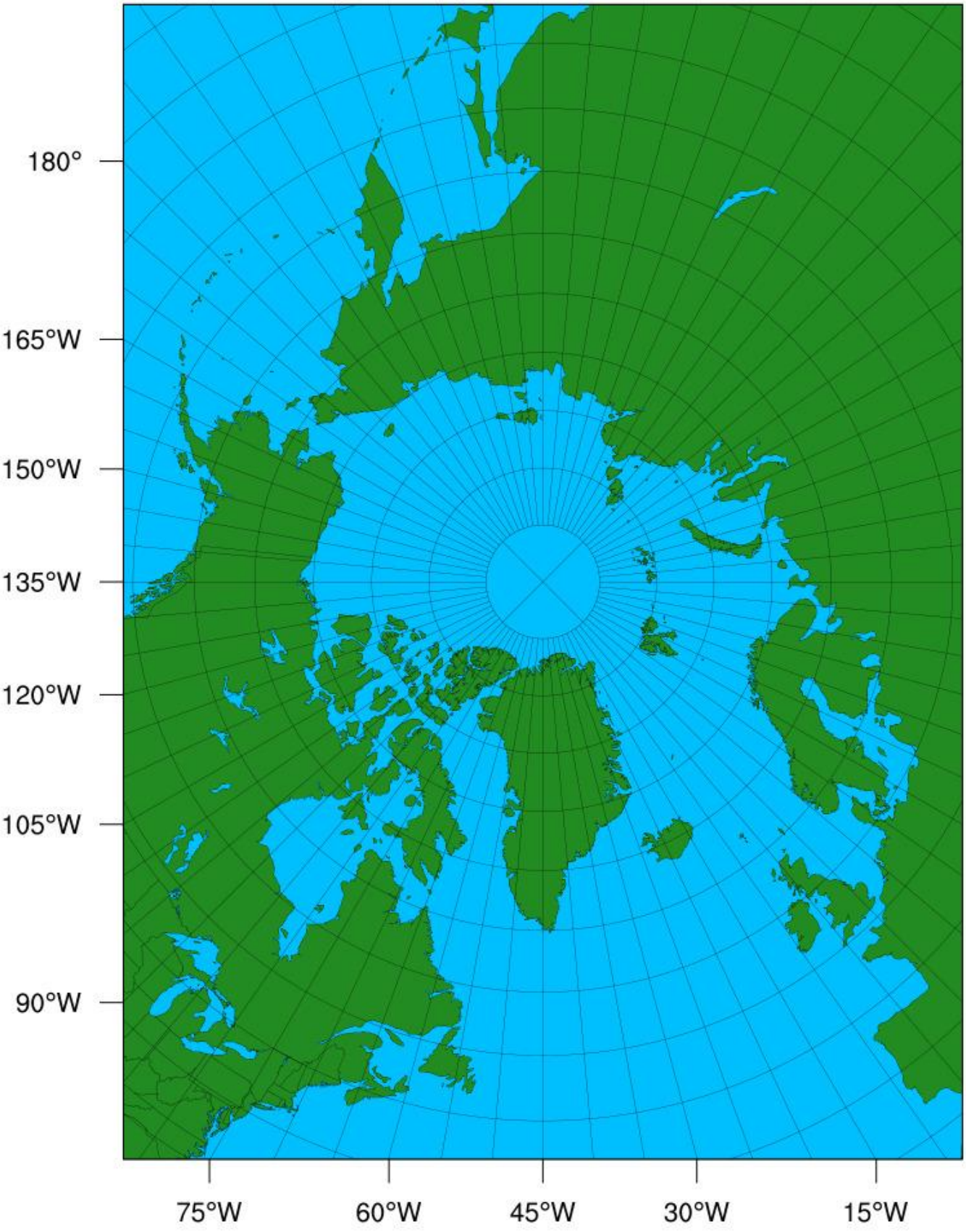

Figure S1 The model domain used in CAPS for pan-Arctic sea ice simulations.

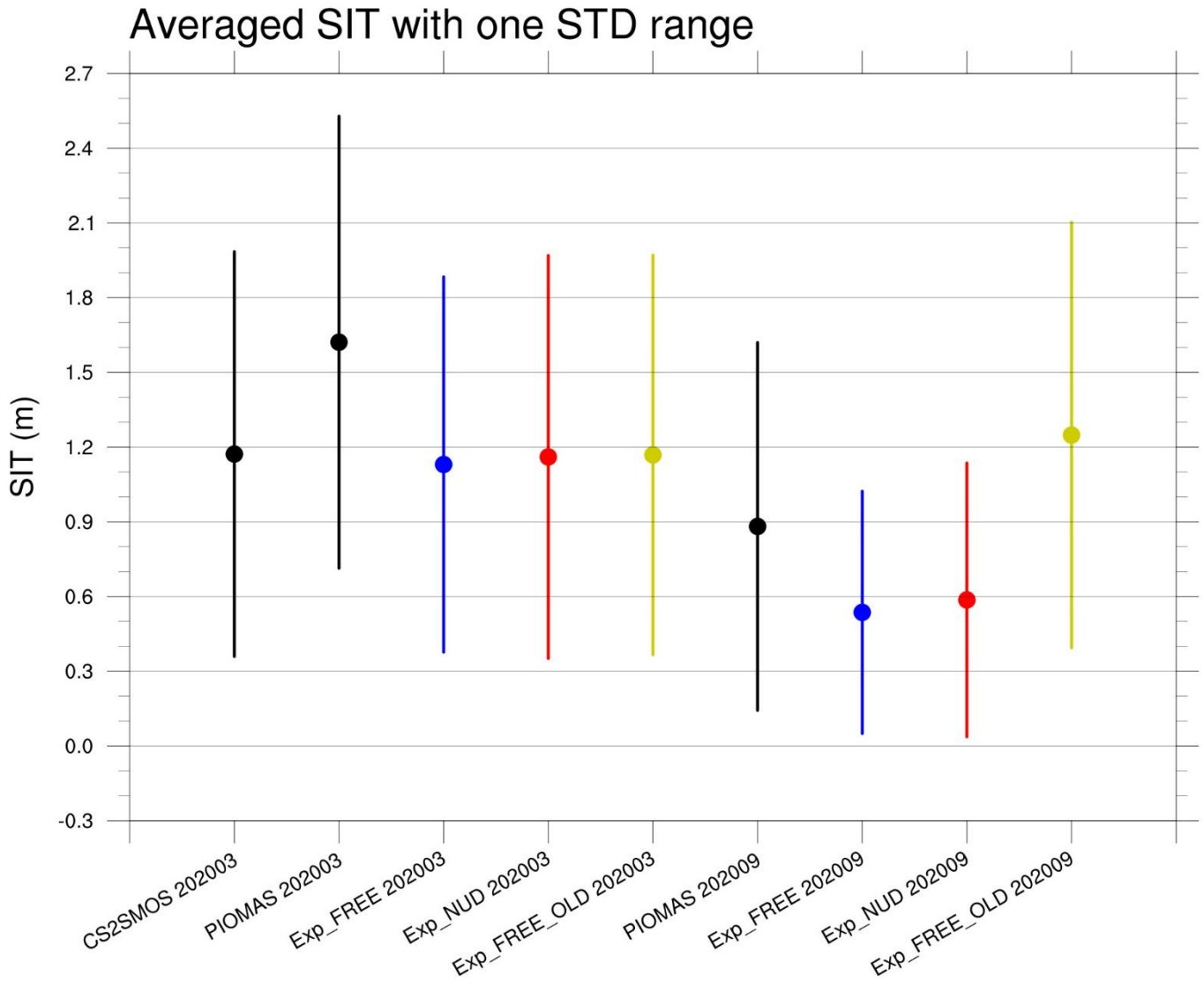

Figure S2 The average sea ice thickness of all cells with at least 1% sea ice concentrations for CS2SMOS, PIOMAS, Exp_FREE, Exp_NUD, and Exp_FREE_OLD in March and September 2020.

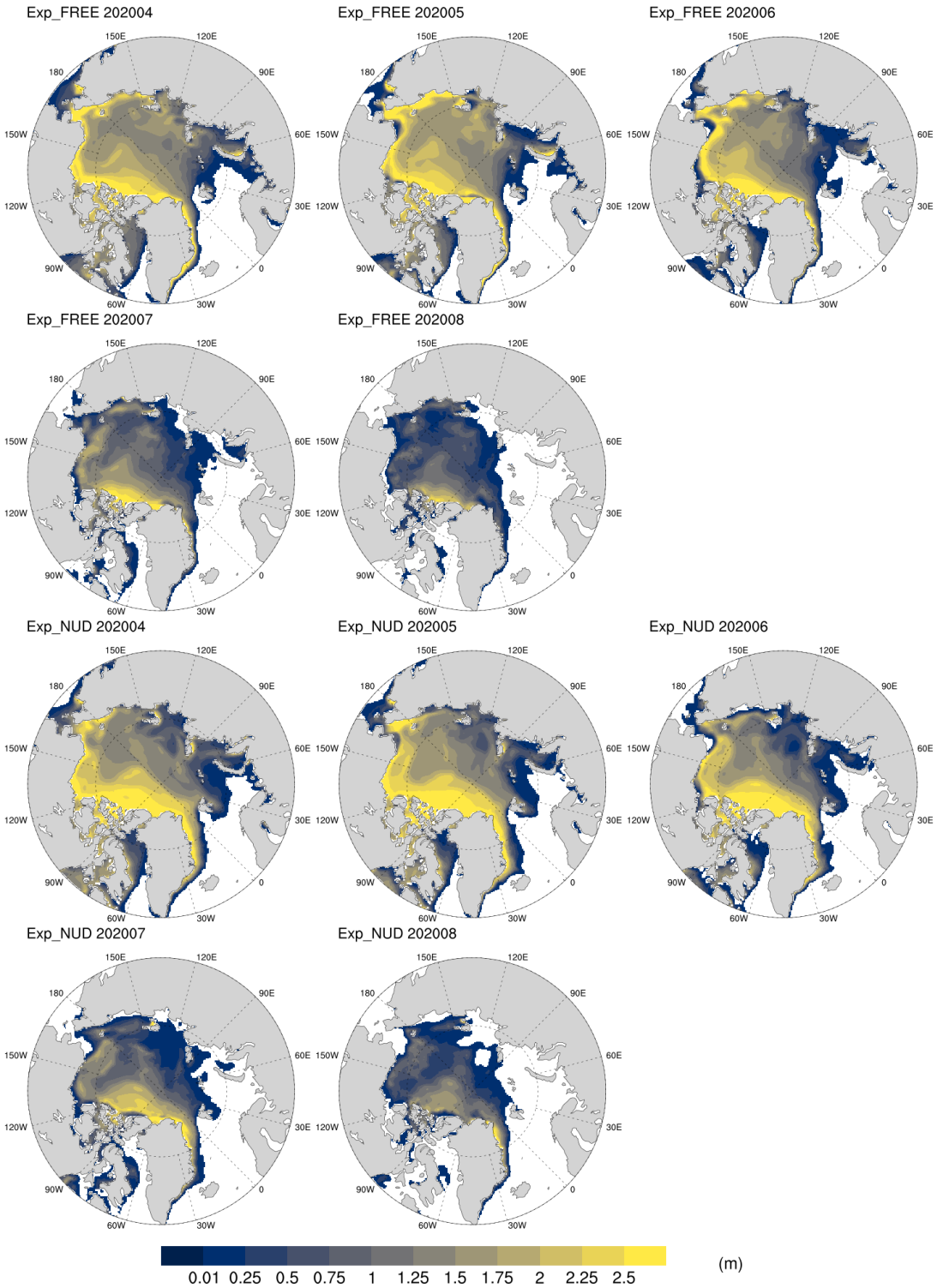

Figure S3 The monthly averaged sea ice thickness of Exp_FREE and Exp_NUD from April 2020 to August 2020.

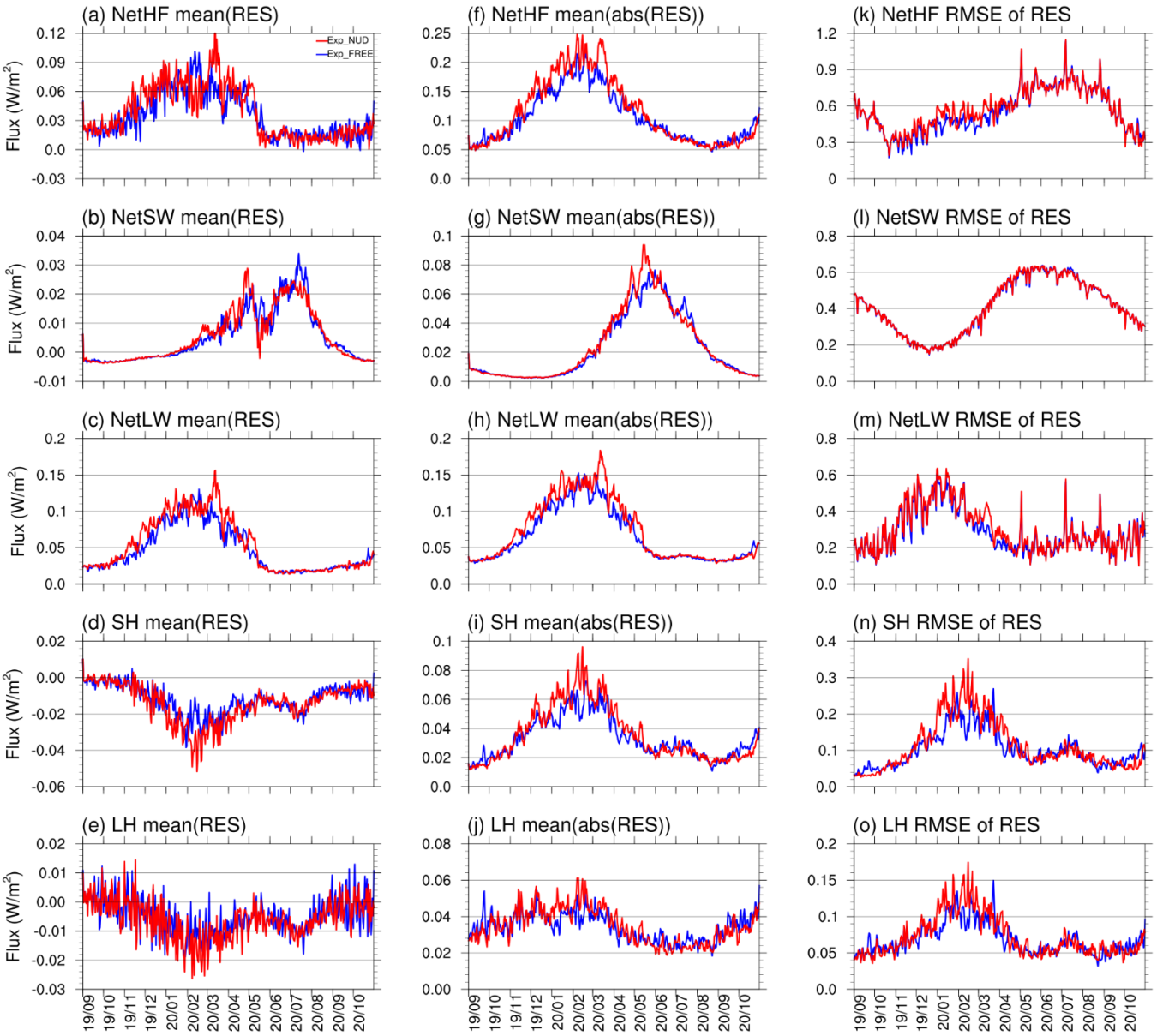

Figure S4 Same as Figure 6, but only for Exp_FREE and Exp_NUD

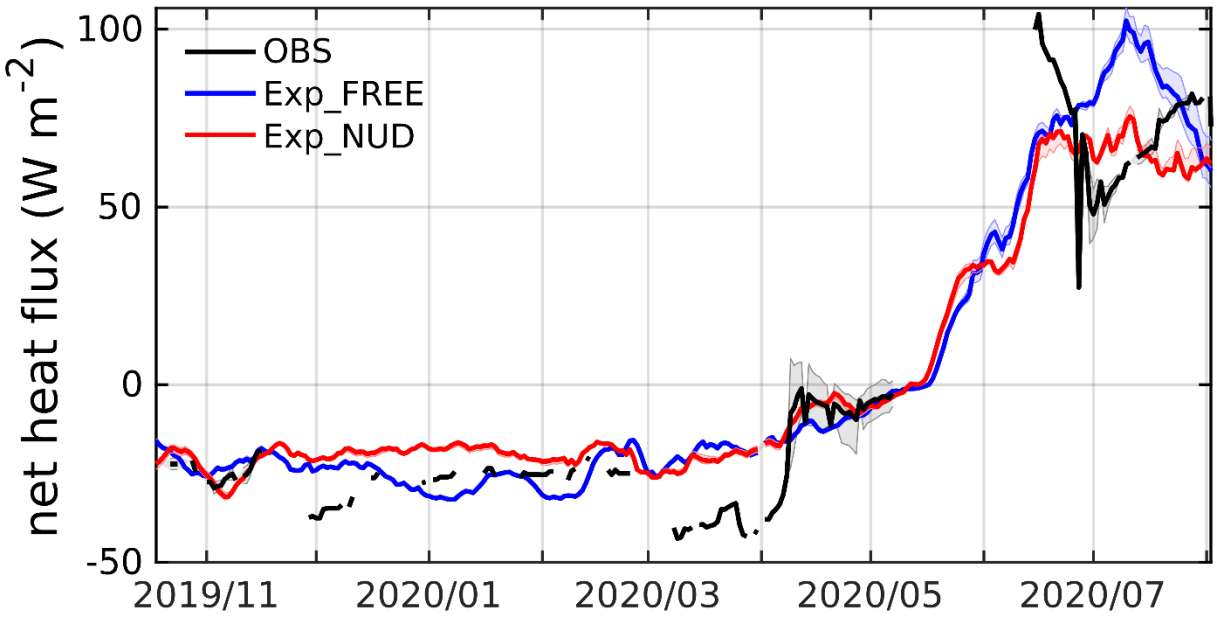

Figure S5 Same as Figure 13, but for net surface heat flux (combining net shortwave, net longwave, sensible, and latent heat fluxes).

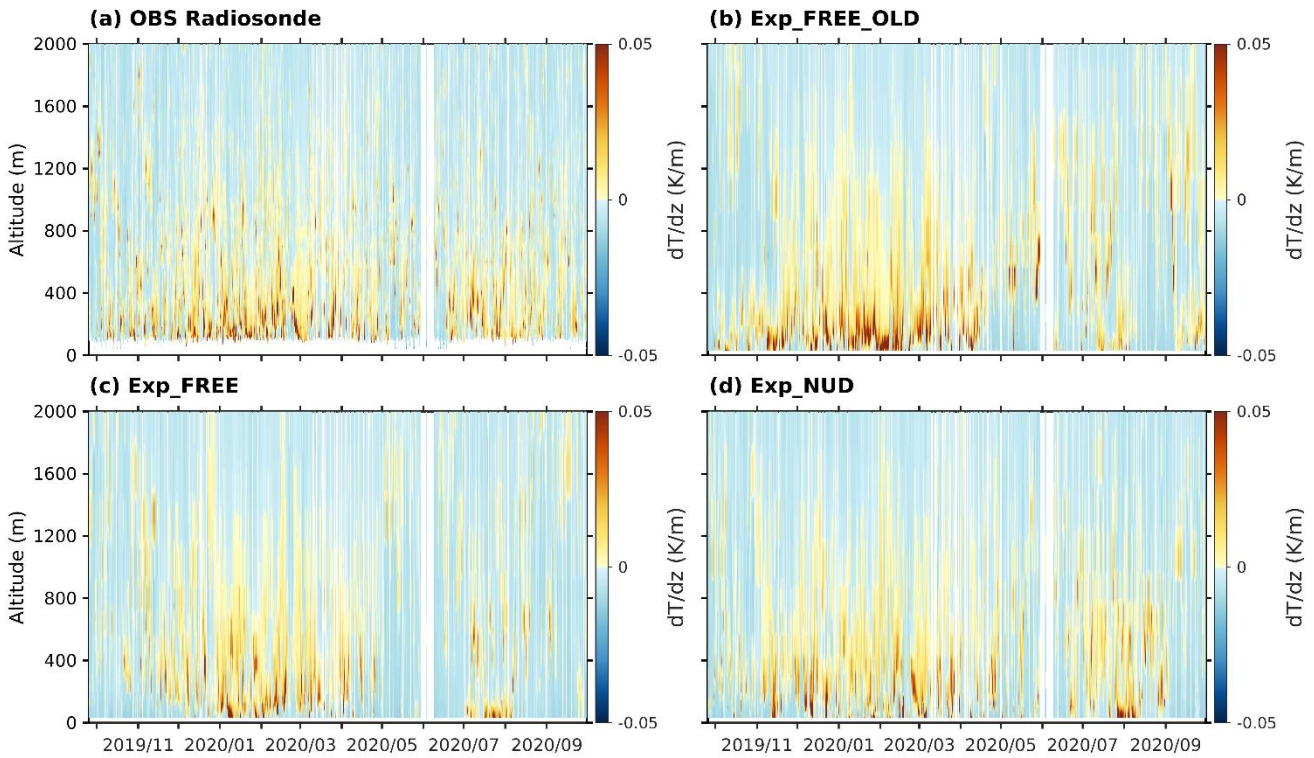

Figure S6 Time-height distributions of temperature lapse rate below 2 km altitude for (a) radiosonde, (b) Exp_FREE_OLD, (c) Exp_FREE, and (d) Exp_NUD along the track of MOSAiC drift.

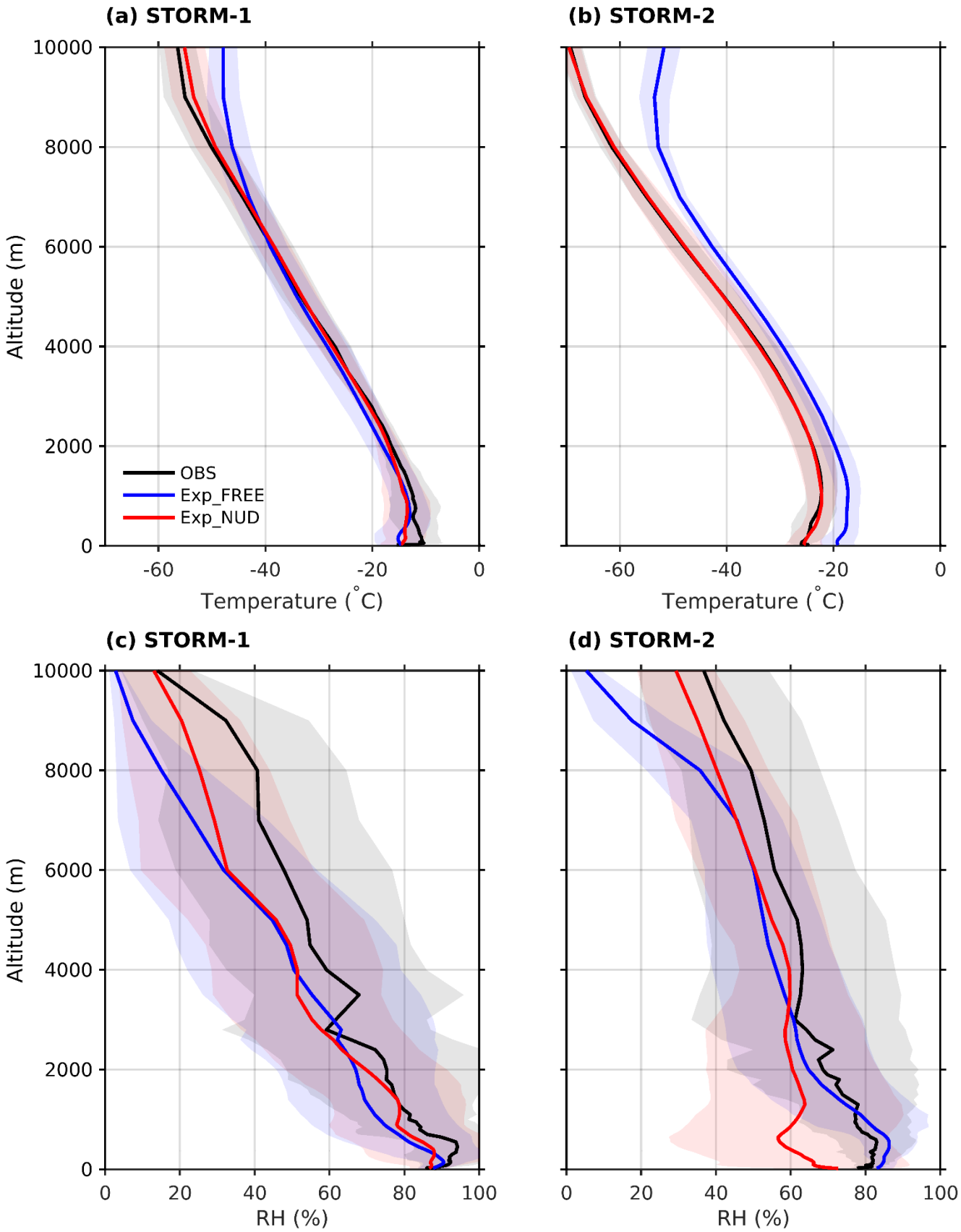

Figure S7 The averaged (a, b) temperature and (c, d) RH profiles for the observations (black line), Exp_FREE (blue line), and Exp_NUD (red line) during the STORM-1 period, and the STORM-2 period. Note: the shading represents one standard deviation range of corresponding variables.

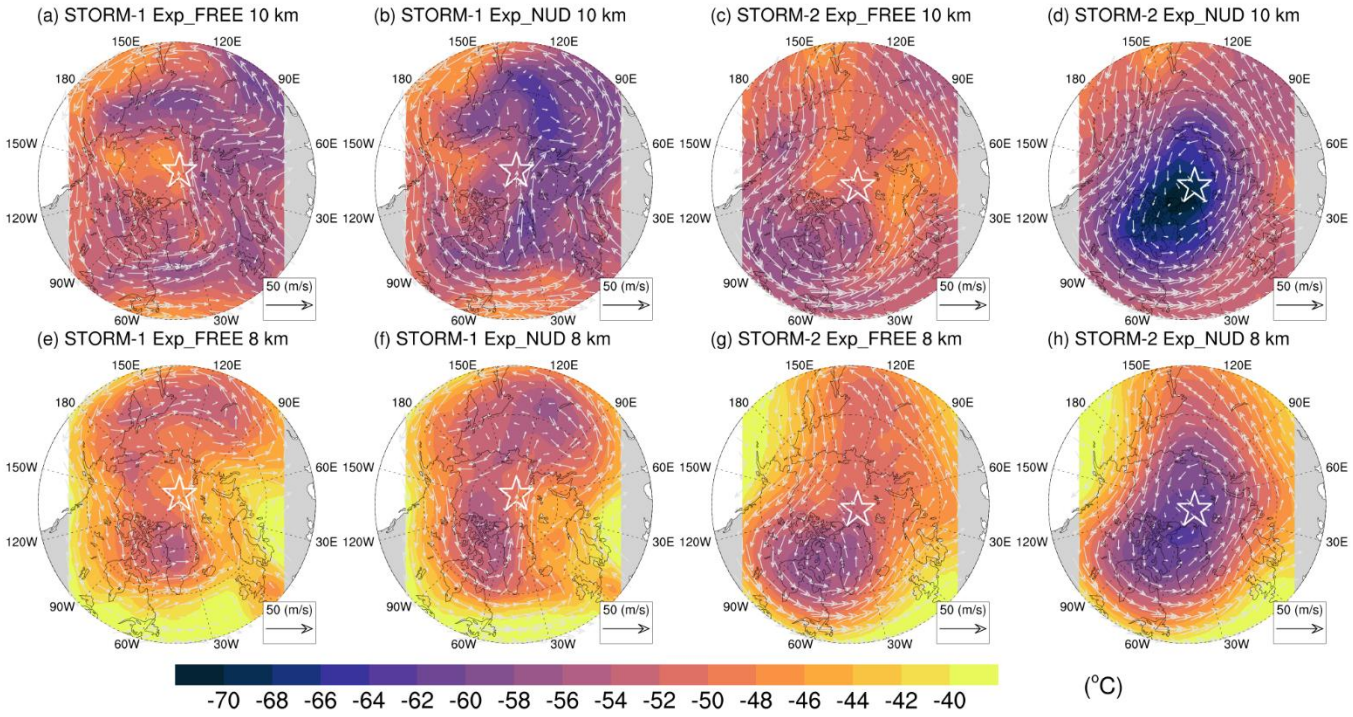

Figure S8 The averaged temperature and wind fields of (a, c, e, g, i, k) Exp_FREE, (b, d, f, h, j, l) Exp_NUD at 10, 9, and 8 km altitude during the STORM-1 and STORM-2 periods. Note: white star represents the averaged location of radiosondes during the STORM-1 and STORM-2 period.

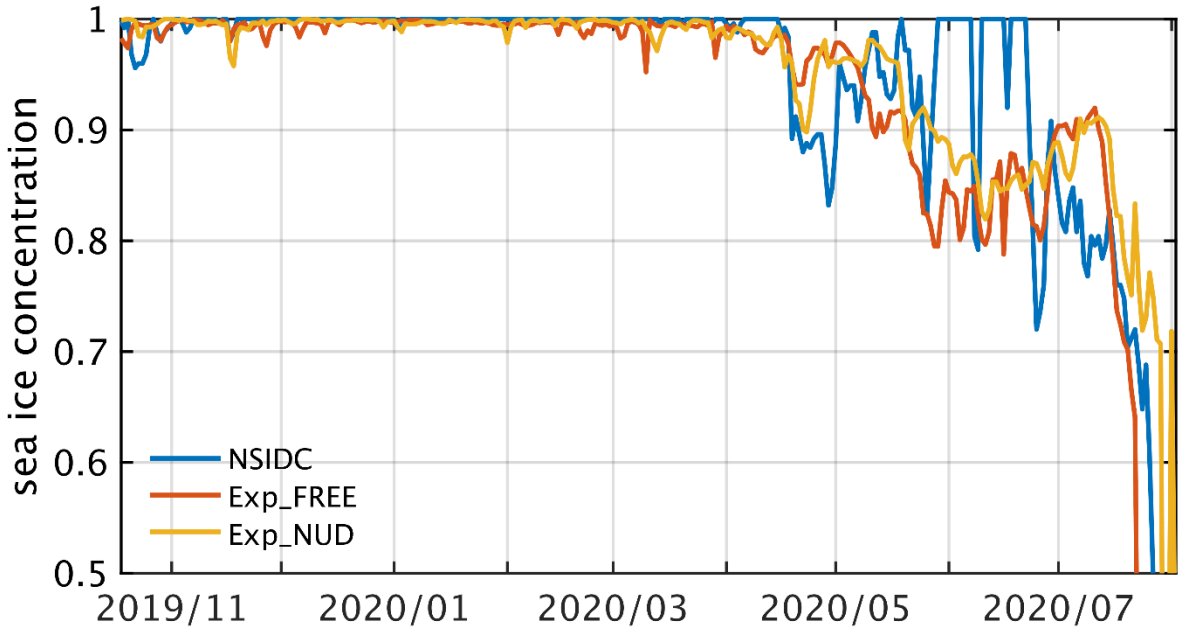

Figure S9 Time-series of sea ice concentration along the track of CTD buoys for the observations, Exp_FREE, and Exp_NUD.

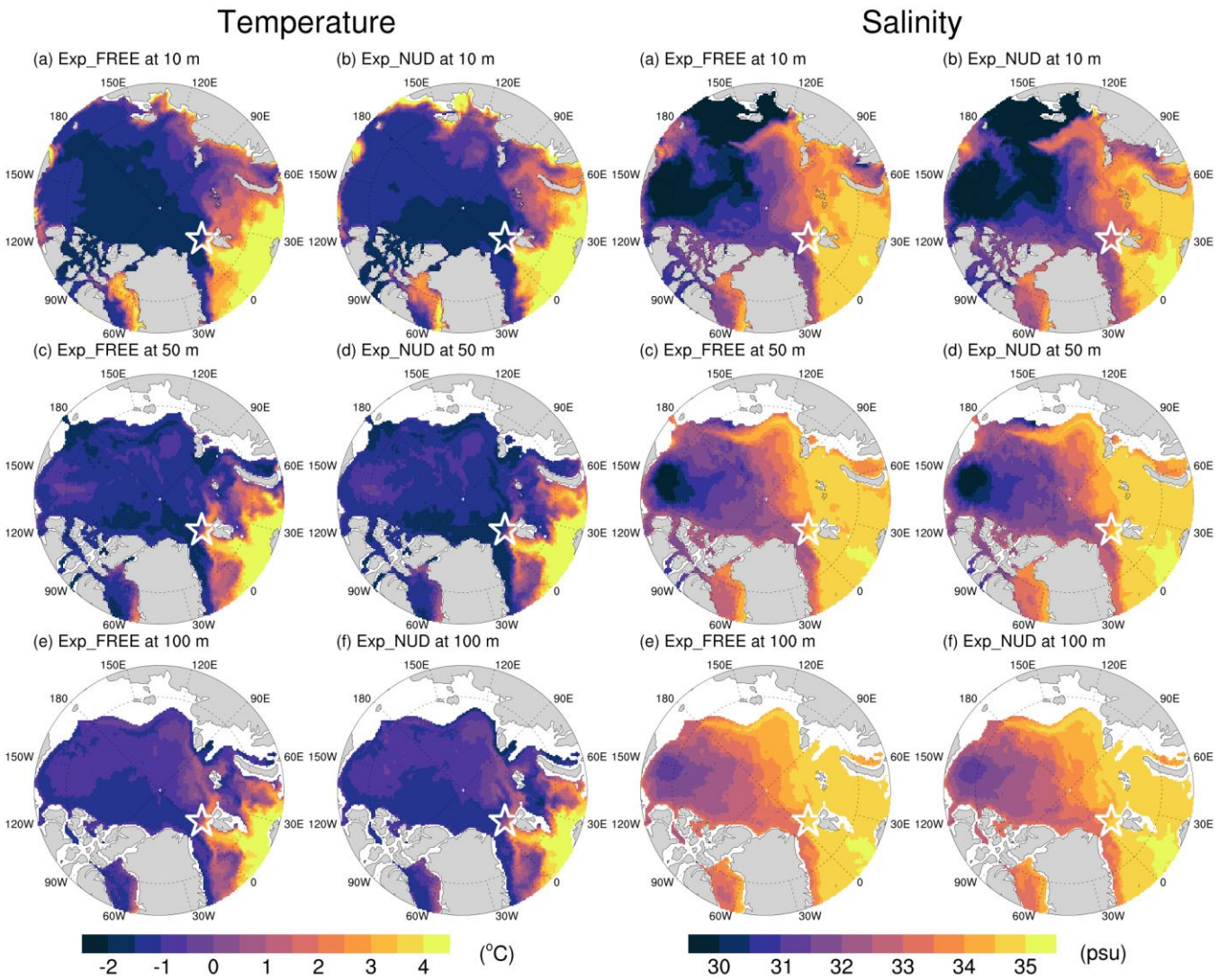

Figure S9 Daily-mean temperature (left panel) and salinity (right panel) of Exp_FREE and Exp_NUD at (a, b) 10, (c, d) 50, and (e, f) 100 m depth on July 1st, 2020. Note: gray star represents the averaged location of CTD buoys.

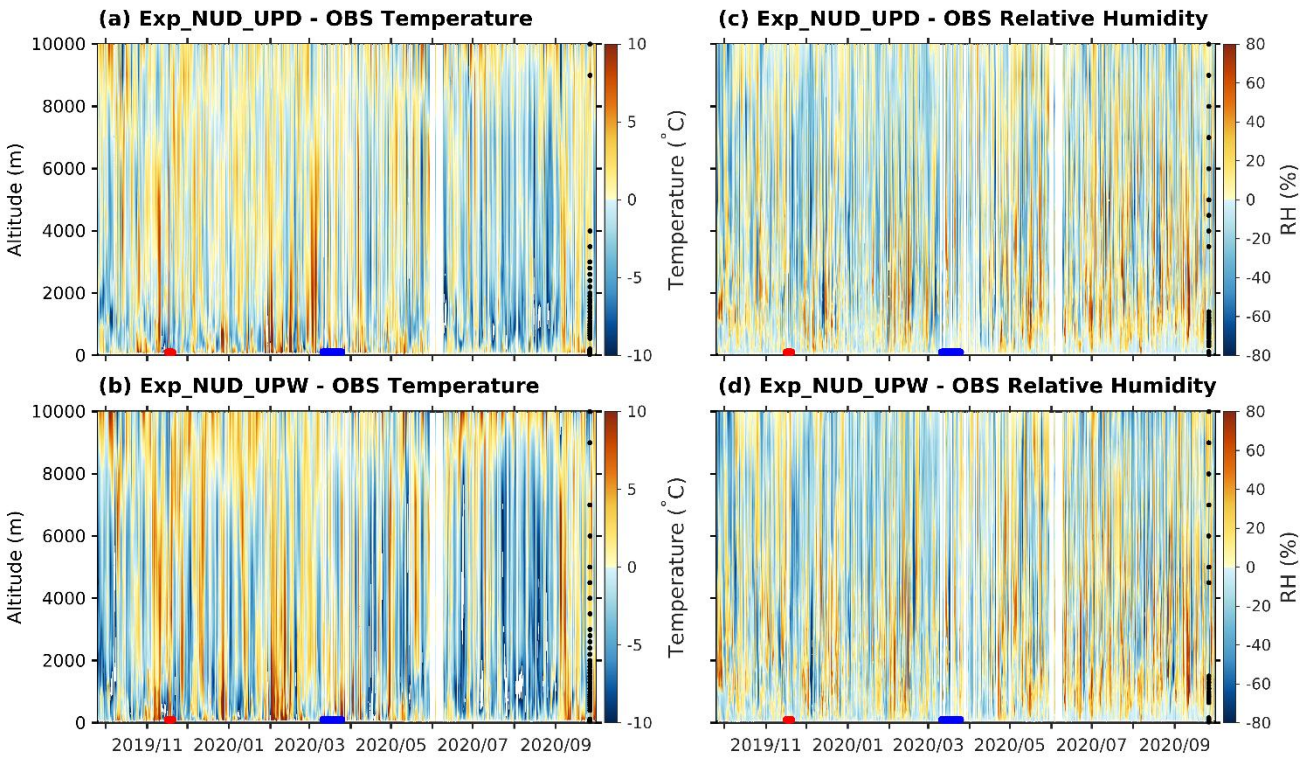

Figure S11 Time-height distributions of simulated temperature biases for (a) Exp_NUD_UPD, and (b) Exp_NUD_UPW, and the RH biases for (c) Exp_NUD_UPD, and (d) Exp_NUD_UPW with respect to the radiosonde observations along the track of MOSAiC drift. Note: red and blue lines on time-axis represent the STORM-1 and STORM-2 periods; black dots near the right edge indicate altitude levels where the full-period mean bias is significantly different from zero based on a pair moving-block bootstrap with 3-day blocks and Benjamini-Hochberg false discovery rate correction at $q = 0.05$. The horizontal position of the black dots is for visualization only and does not correspond to a specific time.

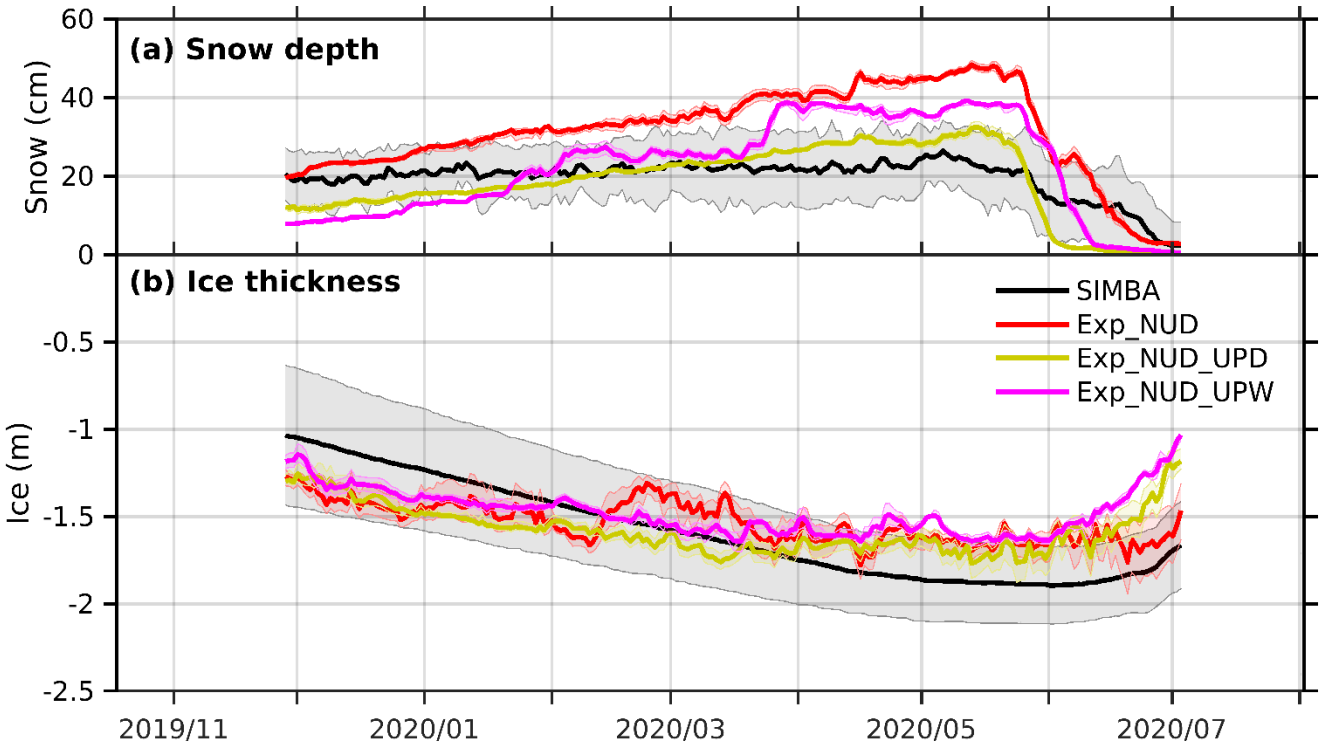

Figure S12 Same as Figure 11, but for Exp_NUD (red line), Exp_NUD_UPD (olive-yellow line), and Exp_NUD_UPW (purple line).

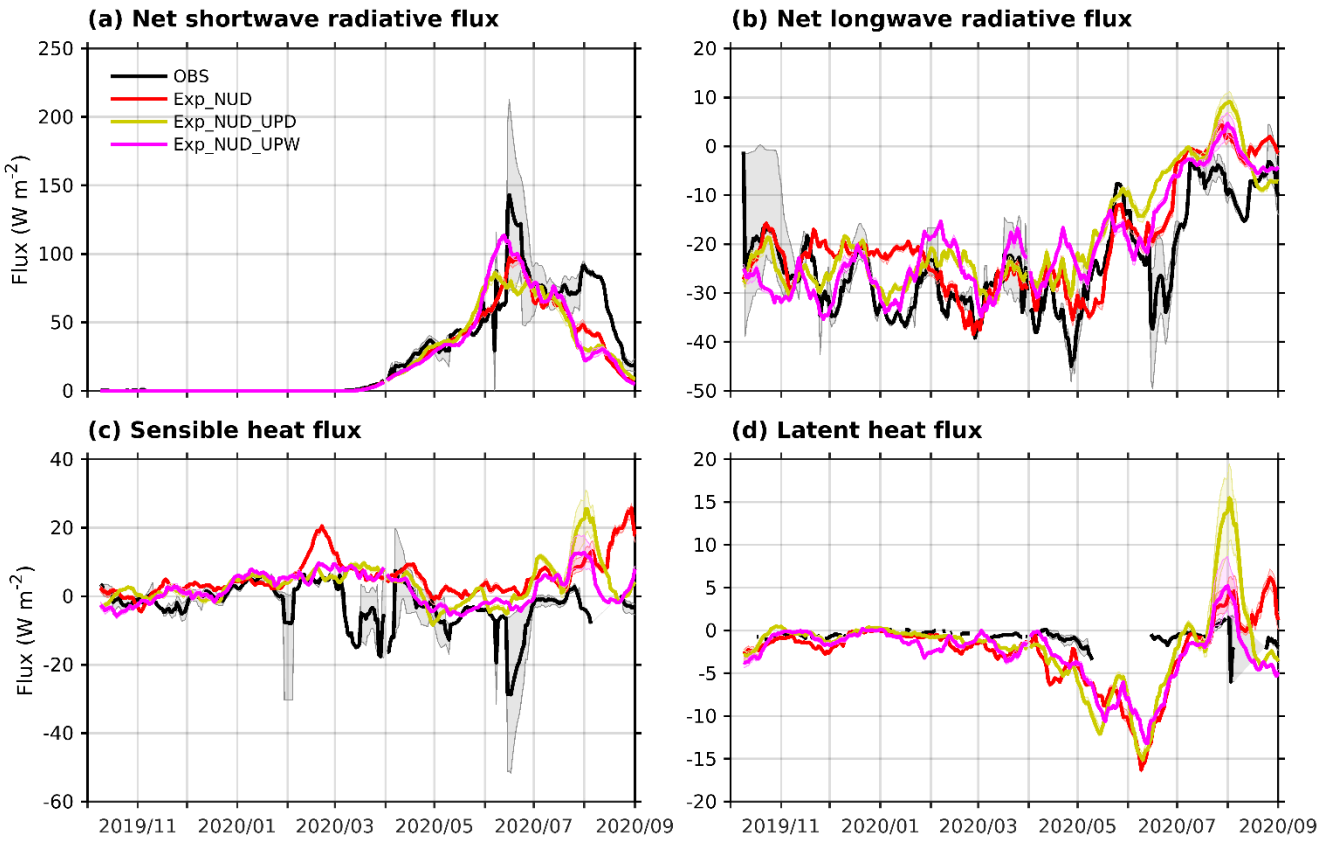

Figure S13 Same as Figure 13, but for Exp_NUD (red line), Exp_NUD_UPD (olive-yellow line), and Exp_NUD_UPW (purple line).